SIAM J. Applied Dynamical Systems
Vol. 1, No. 2, pp. 190–214

A Multiparameter, Numerical Stability Analysis of a Standing Cantilever Conveying Fluid*

Nawaf M. Bou-Rabee†, Louis A. Romero‡, and Andrew G. Salinger‡

Abstract. In this paper, we numerically examine the stability of a standing cantilever conveying fluid in a multiparameter space. Based on nonlinear beam theory, our mathematical model turns out to be replete with exciting behavior, some of which was totally unexpected and novel, and some of which confirm our intuition as well as the work of others. The numerical bifurcation results obtained from applying the Library of Continuation Algorithms (LOCA) reveal a plethora of one, two, and higher codimension bifurcations. For a vertical or standing cantilever beam, bifurcations to buckled solutions (via symmetry breaking) and oscillating solutions are detected as a function of gravity and the fluid-structure interaction. The unfolding of these results as a function of the orientation of the beam compared to gravity is also revealed.

Key words. numerical bifurcation analysis, aero-elasticity, beam flutter, buckling

AMS subject classifications. 74F10, 37M20, 65P30, 74H10

PII. S1111111102400753

1. Introduction.

The dynamics of a standing cantilever conveying fluid has been thoroughly studied for the past century [18]. A major contribution to this problem dates back to 1961 with the work of Benjamin on articulated pipes [4]. Benjamin explained the physical mechanism behind flutter using a theoretical double pendulum model [4]. In a later work, Benjamin shows the destabilizing effect of damping [5].

Païdoussis' experimental and computational work in 1970 confirmed and developed Benjamin's results [15]. Païdoussis' model, based on conservation laws, took into account the flexural restoring force, the fluid inertia force, the gravity force, and the tube inertia force. He also added viscous effects due to external damping.

Using this model, Païdoussis showed that damping does destabilize the beam and that the fluid flow rate can prevent the beam from buckling [15]. In fact, dissipation-induced instabilities have been extensively studied [7], [8] in a wide variety of dynamical systems such

*Received by the editors January 10, 2002; accepted for publication (in revised form) by M. Dellnitz August 5, 2002; published electronically September 12, 2002. This research was supported by Sandia National Laboratories. Sandia is a multiprogram laboratory operated by Sandia Corporation, a Lockheed Martin Company, for the United States Department of Energy under contract DE-AC04-94AL85000. This work was supported by the US DOE through the MICS and ASCI programs. This work was performed by an employee of the U.S. Government or under U.S. Government contract. The U.S. Government retains a nonexclusive, royalty-free license to publish or reproduce the published form of this contribution, or allow others to do so, for U.S. Government purposes. Copyright is owned by SIAM to the extent not limited by these rights.
http://www.siam.org/journals/siads/1-2/40075.html
†California Institute of Technology Applied and Computational Mathematics, 1200 E. California Blvd., MC 217-50, Pasadena, CA 91125 (nawaf@acm.caltech.edu).
‡Sandia National Laboratories, P.O. Box 5800, MS 1110, Albuquerque, NM 87185-1110 (lromero@sandia.gov, agsalin@sandia.gov).

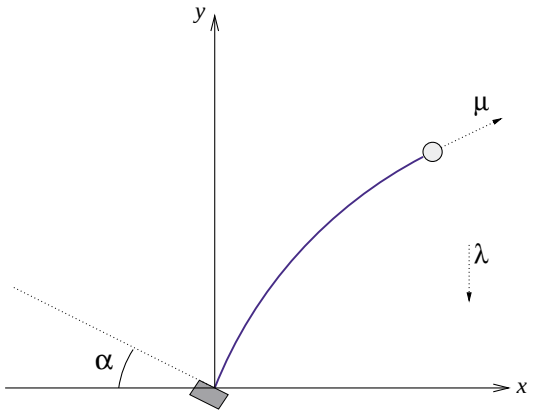

Figure 1.1. *The orientation of the cantilever with respect to gravity (α), the dimension follower force (μ), and the dimensionless gravity (λ) are all parameters in our equations.*

as the double spherical pendulum [13] and rotating systems with gyroscopic terms. Païdoussis also demonstrated using linear theory that there exist a curve of pitchfork bifurcation points and a curve of Hopf bifurcation points in parameter space. The works of Bajaj, Sethna, and Lundgren [1] and Bajaj and Sethna [2], [3] are also noteworthy references on this subject.

In this work, we use a simple model of a standing cantilever conveying fluid, namely, a cantilever beam clamped at one end and free at the other end as shown in Figure 1.1. We assume the fluid-structure interaction induces a concentrated force tangent to the free end of the cantilever and a point source of damping normal to the free end of the cantilever. Our model is simple because we neglect all other fluid structure interaction, including the fluid-induced coriolis forces, unlike the more complete model of Païdoussis [15]. The model is a good representation of a long, thin conduit with a nozzle at its free end. The nozzle maintains the necessary momentum flux, which induces the concentrated force that remains tangent to the free end of the beam. The ratio of the *follower force* to the restoring force due to structural rigidity is denoted as μ, and we will hereafter refer to this quantity as the dimensionless follower force. As we increase μ, the cantilever eventually experiences an oscillatory instability (a Hopf bifurcation). Likewise, the ratio of the gravitational body force to the restoring force due to structural rigidity will be denoted as λ, and we will hereafter refer to this quantity as the dimensionless gravity parameter. Because our model incorporates dimensionless gravity and the beam's orientation to gravity (α), when the standing cantilever is heavy enough, the beam can experience buckling (a pitchfork bifurcation).

This paper extends the results of previous work in several ways. First, we have been able to identify a quartic bifurcation point which more completely maps out the behavior of the beam in parameter space [25]. Second, we have shown analytically, using the perturbation theory of eigenvalues, that damping destabilizes the beam and that, for a point source of damping, the magnitude of damping has no effect on the Hopf bifurcation points. Finally, since we included the inclination of the beam at the clamped end as a parameter in our problem (α), we were able to numerically continue in α. With this capability, we demonstrate how the high codimensional pitchfork bifurcations unfold in α. More precisely, the paper makes the

following assertions supported by numerical evidence and theory:

- When $\alpha = 0.0$, the parameter space is divided by four bifurcation curves: a curve of pitchfork bifurcation points, a curve of Hopf bifurcation points, a curve of turning points, and a curve of saddle-loop bifurcations. We tracked the first three curves presented in section 4.1 using the tracking algorithms in the Library of Continuation Algorithms (LOCA). The theory of the double zero eigenvalue predicts the existence of the saddle-loop bifurcation [12], but we were unable to obtain it using our current capabilities. The saddle-loop bifurcation occurs when a periodic orbit bifurcates to a solution with infinite period.
- When the angle of inclination at the clamped end of the beam is zero ($\alpha = 0.0$), there is a symmetry-breaking Takens–Bogdanov point, where the curve of Hopf bifurcations terminates on a path of pitchfork bifurcations. When we unfold this point in α, it becomes a double zero eigenvalue of codimension two, where the Hopf bifurcation curve terminates at a curve of turning points.
- Again, when $\alpha = 0.0$, there is another extremely degenerate bifurcation point, where the curve of turning points intersects the curve of pitchfork bifurcation points. At this quartic bifurcation point, a symmetry-breaking pitchfork bifurcation changes from supercritical to subcritical [10]. When we unfold this point in α, part of what we get is a codimension two bifurcation, where a curve of turning points terminates at a cusp. We use the theory of normal forms to predict the existence of a curve of turning points in a neighborhood of the quartic bifurcation point and unfold the quartic in section 4.2.
- As expected, a point source of damping had no influence on the stationary bifurcations. Unexpectedly, however, a point source of damping had no influence on the position of the Hopf bifurcation point. Using the perturbation theory of eigenvalues, we will show in section 4.3 why, for a point source of damping, the Hopf bifurcation point is completely independent of the magnitude of damping. This discussion culminates in an explanation of why the beam experiences flutter.

There are also existing techniques for the detection and tracking of bifurcation points. For example, techniques for computing higher codimension Takens–Bogdanov points can be found in [6], [26], and [19]. There is also a large literature on the unfolding of a symmetry-breaking Takens–Bogdanov point [23], [24].

2. Formulation.

2.1. Derivation of equations. The beam has the following properties: length L, mass per unit length ρ, and flexural rigidity EI. We assume that the flexural rigidity about the x-axis is large enough to confine the cantilever beam to move in the x-y plane. The position of the beam is fully described by the vector $\mathbf{X} = (X(s,t), Y(s,t), 0)$, where s is the arclength $s \in [0, L]$ and t is time. The velocity of the beam is given by the vector $\mathbf{V} = (\dot{X}(s,t), \dot{Y}(s,t), 0) = (U(s,t), V(s,t), 0)$. The problem is planar, and we assume that moments are restricted to exist in the z-direction only. Therefore, the moment and force vectors take the following forms: $\mathbf{M} = (0, 0, M_z(s,t))$ and $\mathbf{F} = (F_x(s,t), F_y(s,t), 0)$.

Consider a differential element of the beam of length ds. The forces in the x- and y-directions and bending moment on this differential element are shown in Figure 2.1. A force

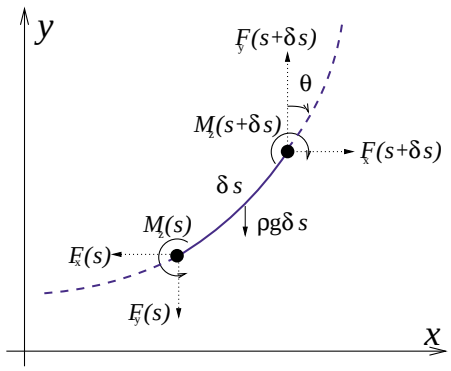

Figure 2.1. *A differential element of the beam.*

balance leads to

$$\rho \frac{\partial^2 X}{\partial t^2} = \frac{\partial F_x}{\partial s},$$
$$\rho \frac{\partial^2 Y}{\partial t^2} = \frac{\partial F_y}{\partial s} - \rho g,$$

and a moment balance results in

$$\left(M_z + \frac{\partial M_z}{\partial s}\, ds \right) - M_z = \mathbf{F} \cdot \mathbf{n}\, ds,$$

where $\mathbf{n}$ is the normal vector defined as

$$\mathbf{n} = (\cos(\theta), -\sin(\theta), 0).$$

The moment is related to the curvature in the following manner:

$$M_z = -EI \frac{\partial \theta}{\partial s}.$$

The negative sign in the moment-curvature relation is due to the definition of θ as being positive moving in the clockwise direction. Using this moment-curvature relation, the moment balance reduces to

$$-EI \frac{\partial^2 \theta}{\partial s^2} = \mathbf{F} \cdot \mathbf{n}.$$

2.2. Governing equations of motion. After including the equations relating the derivatives of X and Y to θ, we obtain a set of five coupled partial differential equations on the

domain $s \in [0, L]$. The dependent variables are F_x, F_y, X, Y, and θ.

$$\begin{aligned} \rho \frac{\partial^2 X}{\partial t^2} &= \frac{\partial F_x}{\partial s}, \\ \rho \frac{\partial^2 Y}{\partial t^2} &= \frac{\partial F_y}{\partial s} - \rho g, \\ 0 &= EI \frac{\partial^2 \theta}{\partial s^2} + \mathbf{F} \cdot \mathbf{n}, \\ 0 &= \frac{\partial X}{\partial s} - \sin\theta, \\ 0 &= \frac{\partial Y}{\partial s} - \cos\theta. \end{aligned} \tag{2.1}$$

The conveying fluid exerts a force on the free end of the beam. We make the reasonable assumption that the follower force remains tangent to the free end of the beam even as the beam moves. Furthermore, the force normal to this follower force contributes to a point source of damping in our model.

$$\begin{aligned} \mathbf{F}(1,t) \cdot \mathbf{t} &= f, \\ -\mathbf{F}(1,t) \cdot \mathbf{n} &= C\mathbf{V}(1,t) \cdot \mathbf{n}, \end{aligned}$$

where C is the damping parameter, f is the follower force, and $\mathbf{t}$ is the tangent vector defined as

$$\mathbf{t} = (\sin(\theta), \cos(\theta), 0).$$

We also assume that the couple at the free end of the beam vanishes. Since the couple is a multiple of the curvature of the beam, this condition reduces to

$$\frac{\partial \theta}{\partial s}(L,t) = 0.$$

On the left side, the beam is clamped, and, at an angle α with respect to gravity,

$$\theta(0,t) = \alpha, \quad X(0,t) = Y(0,t) = 0.$$

Since we will only examine the steady behavior of our governing equations and the linearized behavior about the steady-state, no initial conditions are needed. Together the above equations and boundary conditions are the governing equations of our system.

2.3. Dimensionless equations. We will introduce the dimensionless variables

$$\xi = \tfrac{s}{L}, \quad x = \tfrac{X}{L}, \quad y = \tfrac{Y}{L}, \quad f_x = \tfrac{L^2 F_x}{EI}, \quad f_y = \tfrac{L^2 F_y}{EI}, \quad \tau = \tfrac{\sqrt{EI}}{\sqrt{L^4 \rho}} t.$$

Our dimensionless force and velocity vector take the following forms: $\mathbf{f} = (f_x(\xi,\tau), f_y(\xi,\tau), 0)$ and $\mathbf{v} = (u(\xi,\tau), v(\xi,\tau), 0)$. Substituting these dimensionless variables into (2.1), we have the

equations

$$\begin{aligned} \ddot{x} &= f_x', \\ \ddot{y} &= f_y' - \lambda, \\ 0 &= \theta'' + \mathbf{f}\cdot\mathbf{n}, \\ 0 &= x' - \sin\theta, \\ 0 &= y' - \cos\theta, \end{aligned} \tag{2.2}$$

where the overdot and prime denote differentiation with respect to dimensionless time (τ) and dimensionless arclength (ξ), respectively. In terms of these dimensionless variables, the associated boundary conditions become

$$\begin{gathered} \theta(0,\tau) = \alpha, \qquad x(0,\tau) = y(0,\tau) = 0, \\ -\mathbf{f}(1,\tau)\cdot\mathbf{n} = \gamma\mathbf{v}(1,\tau)\cdot\mathbf{n}, \\ \theta'(1,\tau) = 0, \qquad \mathbf{f}(1,\tau)\cdot\mathbf{t} = \mu, \end{gathered} \tag{2.3}$$

where μ, γ, and λ are the dimensionless follower force, dissipation, and gravity parameters, respectively, and are defined as

$$\mu = \tfrac{fL^2}{EI}, \quad \gamma = \tfrac{\sqrt{EI}}{\sqrt{L^4\rho}}C, \quad \lambda = \tfrac{\rho g L^2}{EI}.$$

We can convert the second-order derivatives in dimensionless time (τ) in (2.2) into first-order derivatives by introducing two additional equations:

$$u = \dot{x}, \quad v = \dot{y}.$$

Then (2.2) can be put into the form

$$\mathbf{M}\dot{\mathbf{z}} = \mathbf{R}(\mathbf{z}), \quad \mathbf{z} \in \Re^n, \tag{2.4}$$

where the vector of unknowns $\mathbf{z}$, the mass matrix $\mathbf{M}$, and the function $\mathbf{R}(\mathbf{z})$ are

$$\mathbf{z} = \begin{bmatrix} x \\ y \\ \theta \\ f_x \\ f_y \\ u \\ v \end{bmatrix}, \quad \mathbf{M} = \begin{bmatrix} 0 & 0 & 0 & 0 & 0 & 1 & 0 \\ 0 & 0 & 0 & 0 & 0 & 0 & 1 \\ 0 & 0 & 0 & 0 & 0 & 0 & 0 \\ 0 & 0 & 0 & 0 & 0 & 0 & 0 \\ 0 & 0 & 0 & 0 & 0 & 0 & 0 \\ 1 & 0 & 0 & 0 & 0 & 0 & 0 \\ 0 & 1 & 0 & 0 & 0 & 0 & 0 \end{bmatrix}, \quad \mathbf{R}(\mathbf{z}) = \begin{bmatrix} f_x' \\ f_y' - \lambda \\ \theta'' + \mathbf{f}\cdot\mathbf{n} \\ x' - \sin\theta \\ y' - \cos\theta \\ u \\ v \end{bmatrix}.$$

In this paper, we never analyze the transient dynamics of (2.4). Instead, we look for equilibrium solutions $\bar{\mathbf{z}}$ of (2.4) which satisfy

$$\mathbf{R}(\bar{\mathbf{z}}) = \mathbf{0}.$$

The stability of this solution can be determined by linearizing (2.4) about $\bar{\mathbf{z}}$. After substituting an expansion of $\bar{\mathbf{z}}$ ($\bar{\mathbf{z}} + \bar{\mathbf{z}}_\mathbf{1}$) into (2.4), we obtain the linear system

$$\mathbf{M}\dot{\bar{\mathbf{z}}}_\mathbf{1} = \mathbf{R}_\mathbf{z}(\bar{\mathbf{z}})\bar{\mathbf{z}}_\mathbf{1},$$

where $\mathbf{R_z}(\bar{\mathbf{z}})$ is the Fréchet derivative.

Substituting $\bar{\mathbf{z}}_\mathbf{1} = e^{\sigma t}\phi$ into the linearized system, we obtain

$$\sigma \mathbf{M}\phi = \mathbf{R_z}(\bar{\mathbf{z}})\phi. \tag{2.5}$$

Equation (2.5) is a generalized eigenvalue problem for the continuous problem with eigenfunction ϕ and eigenvalue σ. If all of the eigenvalues of our eigenvalue problem have negative real parts, the equilibrium solution $\bar{\mathbf{z}}$ is stable.

2.4. Linearization about standing cantilever. Equation (2.4) may not be familiar to readers with a background in beam theory. Linearizing, however, about the standing cantilever solution would result in a set of equations that more closely resembles the set of equations from beam theory. We simply evaluate the Fréchet derivative at the standing cantilever fixed point ($f_x = 0,\ f_y = -\mu+\lambda(s-1),\ x = 0,\ y = s$) in (2.5). After manipulating the resulting set of equations, we obtain a fourth-order differential equation in x. The stability of the standing cantilever fixed point is determined from the eigenvalues of the resulting linear operator

$$L(\phi) = \phi'''' - (((s-1)\lambda - \mu)\phi')' = -\sigma^2\phi \tag{2.6}$$

with the associated boundary conditions

$$\phi(0) = \phi'(0) = 0, \quad \phi''(1) = 0, \quad \phi'''(1) = \gamma\sigma\phi. \tag{2.7}$$

This linear operator has several interesting properties. First, L is not self-adjoint because of the boundary condition at the free end: $\phi'''(1) = \gamma\sigma\phi$. If we made a tiny change in this boundary condition,

$$\phi'''(1) + \mu\phi'(1) = 0,$$

the linear operator would be self-adjoint. This boundary condition change would result in a linear operator which represents the classical equations describing the buckling of a beam.

If $\gamma = 0$, the linear operator L exhibits time-reversal symmetry since, if σ is an eigenvalue of this linear operator, then so is $-\sigma$. The linear operator is also non-self-adjoint when $\gamma = 0$. Because of time-reversal symmetry, the eigenvalues of the linear operator for the undamped case indicate only neutral stability or instability. Numerically, we have determined (with $\alpha = 0$) that the beam loses neutral stability when $\mu = 20$. When a small amount of damping γ is introduced, however, the beam loses stability when $\mu = 16$. This apparent paradox was noted by Païdoussis [15] and will be explained in section 4.3.

We will need the adjoint eigenvalue problem when we apply the perturbation theory of eigenvalues in section 4.3. For the purpose of computing this adjoint, we will define the following inner product:

$$\langle f, g\rangle = \int_0^1 f^* g(s) ds,$$

where f^* is the complex conjugate of f. Since we will deal exclusively with real eigenfunctions in the neutrally stable regime, we will drop the complex conjugate notation. The adjoint of our linear operator L^* satisfies the following inner product:

$$\langle \psi, L(\phi)\rangle = \langle L^*\psi, \phi\rangle.$$

Taking the inner product of an arbitrary function ψ with the linear operator in (2.6), we obtain

$$\langle \psi, L(\phi) \rangle = \int_0^1 \psi(\phi'''' - ((\lambda(s-1) - \mu)\phi')')ds.$$

We can obtain the adjoint linear operator by repeatedly integrating this equation by parts to obtain

$$\begin{aligned}\langle \psi, L(\phi) \rangle = \int_0^1 \phi(\psi'''' - ((\lambda(s-1) - \mu)\psi')')ds + \psi\phi'''\big|_0^1 - \psi'\phi''\big|_0^1 \\ + \ \psi''\phi'\big|_0^1 - \psi'''\phi\big|_0^1 + \psi((\lambda(s-1) - \mu)\phi')'\big|_0^1 - \psi'(\lambda(s-1) - \mu)\phi'\big|_0^1.\end{aligned}$$

Several of these terms evaluated at the boundaries vanish due to the boundary conditions on ϕ except

$$\begin{aligned}\mu(\psi(1)\phi'(1) - \psi'(1)\phi(1)) - \psi'''(1)\phi(1) \\ + \psi''(1)\phi'(1) + \psi''(1)\phi'(1) + \psi'(0)\phi''(0) + \psi(0)\phi'''(0).\end{aligned}$$

We will specify the boundary conditions of the adjoint eigenvalue problem so that these terms vanish as well:

$$\begin{aligned}\psi(0) = \psi'(0) = 0, \\ \psi'''(1) + \mu\psi'(1) = 0, \\ \psi''(1) + \mu\psi(1) = 0.\end{aligned}$$

The adjoint eigenvalue problem follows:

$$L^*(\psi) = \psi'''' - (((s-1)\lambda - \mu)\psi')' \tag{2.8}$$

with the boundary conditions

$$\begin{aligned}\psi(0) = \psi'(0) = 0, \\ \psi'''(1) + \mu\psi'(1) = 0, \\ \psi''(1) + \mu\psi(1) = 0.\end{aligned} \tag{2.9}$$

This adjoint linear operator will be useful when we examine the effects of damping on stability in section 4.3.

3. Numerical technique. We approximated the derivatives that appear in the steady form of (2.4) using a Chebyshev collocation method. The approximating functions employed by this spectral method are Chebyshev polynomials which are infinitely differentiable global functions. When evaluated at the Gauss–Labotto points, this spectral method produces highly accurate approximations to the derivative [9].

We computed the steady-state solutions of our discrete approximation to (2.4) using a Newton–Raphson iteration,

$$\mathbf{R}_\mathbf{z}(\mathbf{z_o})\delta\mathbf{z} = -\mathbf{R}(\mathbf{z_o}),$$

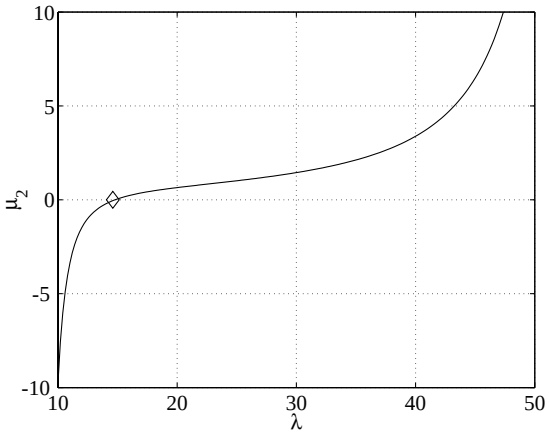

Figure 3.1. *This plot of μ_2 as a function of λ shows that μ_2 changes sign at approximately $\mu = 7.3447$ and $\lambda = 14$. The variation of the solution as a function of λ at this transition point (marked with a diamond) is shown in bifurcation diagram* (b) *in Figure 4.4. This transition point is called a quartic bifurcation point and is invariant under a change in the parameterization.*

where $\mathbf{z_o}$ is the solution at the previous iteration, $\delta\mathbf{z}$ is the update to $\mathbf{z_o}$ for this iterate, and $\mathbf{R_z}(\mathbf{z_o})$ is the Fréchet derivative. We also approximated the continuous eigenvalue problem in (2.4) with a discrete approximation to the Fréchet derivative, the vector of unknowns $\bar{\mathbf{z}}$, and the eigenfunction ϕ.

We used the arclength continuation, Hopf, pitchfork, and turning point tracking algorithms in LOCA to obtain the numerical bifurcation results in this paper. For more information on these algorithms, consult [14], [20], [21]. Branch switching was accomplished using an algorithm which perturbs the symmetric, unstable solution in the direction of the null vector, ϕ:

$$\mathbf{z}_{stable} = \mathbf{z}_{unstable} + \frac{\phi}{||\phi||}.$$

The transition from a supercritical to a subcritical pitchfork bifurcation can be determined using bifurcation theory. Werner and Spence discuss an analogous approach to detect whether a pitchfork bifurcation is supercritical or subcritical in [25]. We first transform our governing equations so that $\mathbf{z} = \mathbf{0}$ is the standing cantilever solution. We then introduce a regular perturbation expansion about $\mathbf{z_0} = \mathbf{0}$ to third order in ϵ. Let us choose as our bifurcation parameter the dimensionless follower force μ. We also expand this bifurcation parameter as follows:

$$\mu = \mu_0 + \epsilon\mu_1 + \epsilon^2\mu_2 + \epsilon^3\mu_3.$$

We substitute these expansions into our equations and retain terms up to third order in ϵ. If we were to collect terms of first order in ϵ, we obtain the eigenvalue problem at the bifurcation point:

$$\mathbf{J}(0, \mu_0)\mathbf{z_1} = 0.$$

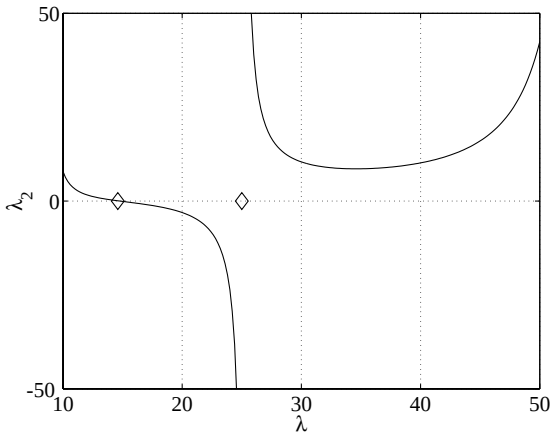

Figure 3.2. *This plot of λ_2 as a function of λ shows that there are two points (marked with diamonds) where λ_2 changes sign. The point that is also predicted in Figure 3.1 is special because it is invariant under a change in the parameterization, whereas the second point predicted when λ is chosen as the bifurcation parameter is an artifact of the parameterization we take but still accurately predicts a change in the criticality of the pitchfork bifurcation.*

Collecting terms of second order in ϵ, we obtain an equation of the form

$$\mathbf{J}(\mathbf{0}, \mu_0)\mathbf{z_2} + \mu_1\beta = \mathbf{Q}(\mathbf{z_1}).$$

Finally, collecting terms of third order in ϵ, we obtain an equation of the form

$$\mathbf{J}(\mathbf{0}, \mu_0)\mathbf{z_3} + \mu_2\beta = \mathbf{C}(\mathbf{z_1}, \mathbf{z_2}).$$

We also have the normalization condition, which provides a nontrivial solution to these equations:

$$\phi \cdot \mathbf{z_k} = 0, \quad k = 1, 2.$$

By solving the following system of equations simultaneously for $\mu_{k-1}, k = 1, 2$, we can obtain the sign of μ_2:

$$\begin{bmatrix} \mathbf{J}(0, \mu_0) & \beta \\ \phi & 0 \end{bmatrix} \begin{bmatrix} \mathbf{z_k} \\ \mu_{k-1} \end{bmatrix} = \begin{bmatrix} \mathbf{R}(\mathbf{z_{k-1}}) \\ 0 \end{bmatrix}.$$

The pitchfork bifurcation is supercritical or subcritical based on the sign of μ_2. We solved these equations numerically and obtained the transition point (for $\alpha = 0$) at $\mu = 7.3447$, as seen in bifurcation diagram (b) in Figure 4.4. The variation of μ_2 as a function of λ is shown in Figure 3.1. If we were to choose the dimensionless gravity λ as our bifurcation parameter, we obtain two points where λ_2 changes sign once through 0 and once through ∞. The first transition point is the quartic bifurcation point, which is invariant under a change in the parameterization. The second transition point is an artifact of the parameterization we chose but is nonetheless a meaningful indicator of the change in criticality. A plot of λ_2 as a function of λ is shown in Figure 3.2.

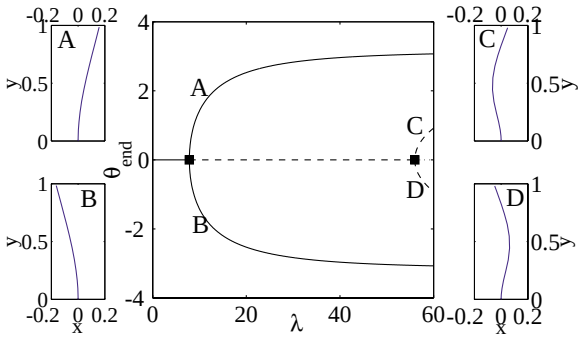

Figure 4.1. *The full and dashed lines represent stable and unstable solutions, respectively, and the square marker indicates a pitchfork bifurcation point. The symmetric solution is unstable past the pitchfork bifurcation point and tends toward the two stable branches labeled* A *and* B *in the diagram. Sample bifurcated solutions are shown.* A *and* B *correspond to the first unstable mode, and* C *and* D *correspond to the second unstable mode. The standing cantilever fixed point, not shown, corresponds to the horizontal* $\theta = 0$ *branch.*

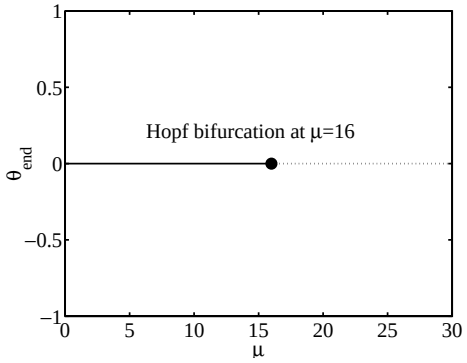

Figure 4.2. *The full and dotted lines represent stable and doubly unstable solutions, respectively. The value of* μ *at the onset of oscillatory behavior is shown in this figure.*

4. Results and analysis.

4.1. Numerical bifurcation results. Figure 1.1 illustrates the beam's orientation as we vary α. When $\alpha = 0$, the standing cantilever is a solution for all parameter values, but it may not be stable to small perturbations. In this section, we will explore the standing cantilever's stability in the parameter plane defined by λ and μ when the underlying equations of the beam exhibit reflectional symmetry $\alpha = 0.0$.

Consider the case when there is no follower force or $\mu = 0.0$. When gravity is pointing toward the clamped end of the beam, the standing cantilever will buckle under its own weight at a critical value of λ. As in the Euler beam problem, the standing cantilever will also have a second mode of instability at another critical value of λ. These points of instability are shown in Figure 4.1 with sample buckled solutions. This stationary bifurcation point is characterized as being supercritical since the branched solutions are stable and occur after the symmetric solution loses stability. Now consider the case when $\lambda = 0.0$. The beam experiences flutter at a critical value of the dimensionless follower force μ. This dynamic instability corresponds to

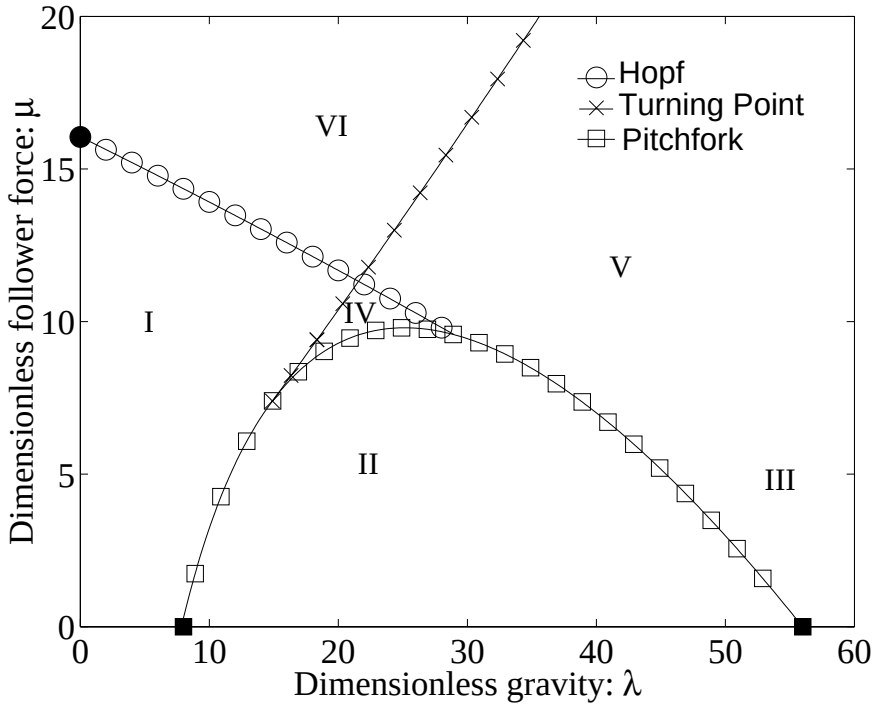

I. one symmetric solution — II. two buckled solutions
III. two buckled solutions — IV. one symmetric and two buckled solutions
V. one oscillatory solution — VI. oscillatory and buckled solutions

Figure 4.3. *For $\alpha = 0.0$ and $\gamma = 1.0$. Each region indicated with a Roman numeral and demarcated by the curves of bifurcation points has different stable solutions defined above. This two-parameter plot shows all solutions in this parameter-space. Please view Figure 4.4 for a better understanding of how the solutions vary as a function of μ and λ. Note that this figure contains two different bifurcation boundaries: one from the trivial state (the curve of pitchfork and Hopf bifurcations) and the other from an already buckled state (the curve of turning points).*

a Hopf bifurcation point and is shown in Figure 4.2. The dotted line in the figure represents an unstable solution which tends to an oscillatory solution. Since we know the bifurcations that the beam experiences for the trivial cases when $\mu = 0.0$ and $\lambda = 0.0$, we can use the tracking capabilities in LOCA to obtain the curve of pitchfork and Hopf bifurcation points.

As seen in Figure 4.3, the curve of pitchfork bifurcation points and the curve of Hopf bifurcation points intersect at a point which is a high codimension bifurcation. This point appears to be accounted for by Païdoussis in his stability map of the boundaries of buckling and oscillatory instabilities [15]. His stability map, however, misses the quartic bifurcation point, which we were able to obtain using an algorithm discussed in section 3 that detects whether a pitchfork bifurcation point is supercritical or subcritical.

By using this additional capability, we can obtain the quartic bifurcation point shown in Figure 4.3. This point is another a high codimension bifurcation point. Using the theory of normal forms, we show in section 4.2 that another curve of turning points should come tangent to this curve. This conclusion based on theory inspired us to search for the curves of turning

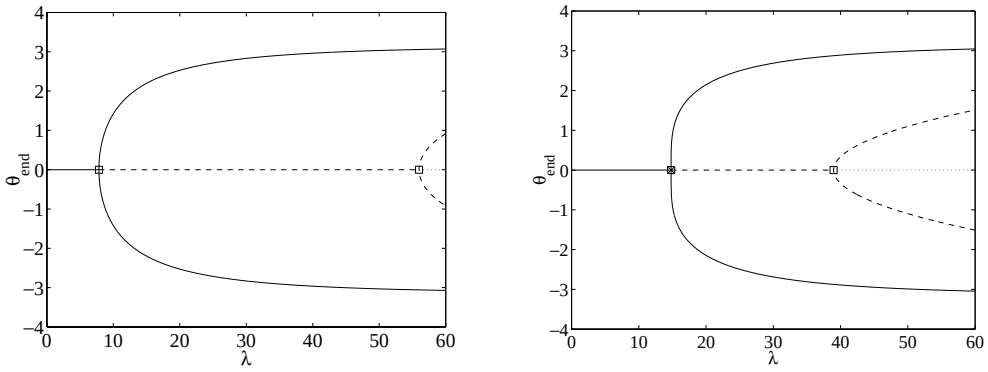

(a) $\mu = 0.0$ (b) $\mu = 7.3447$

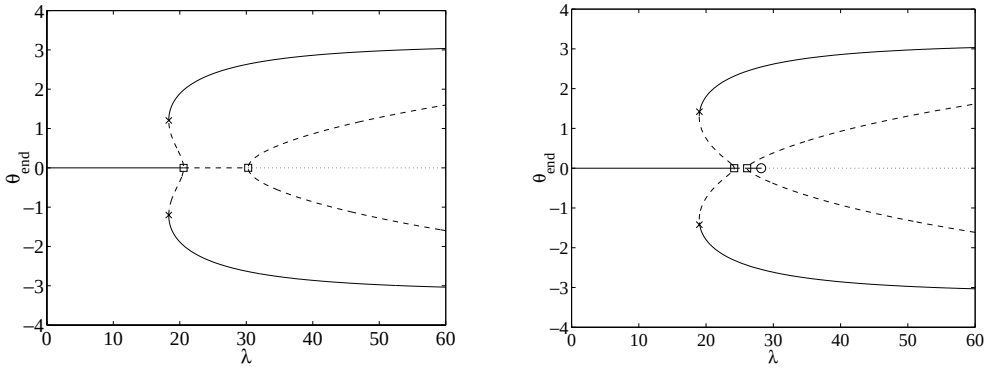

(c) $\mu = 9.4$ (d) $\mu = 9.78$

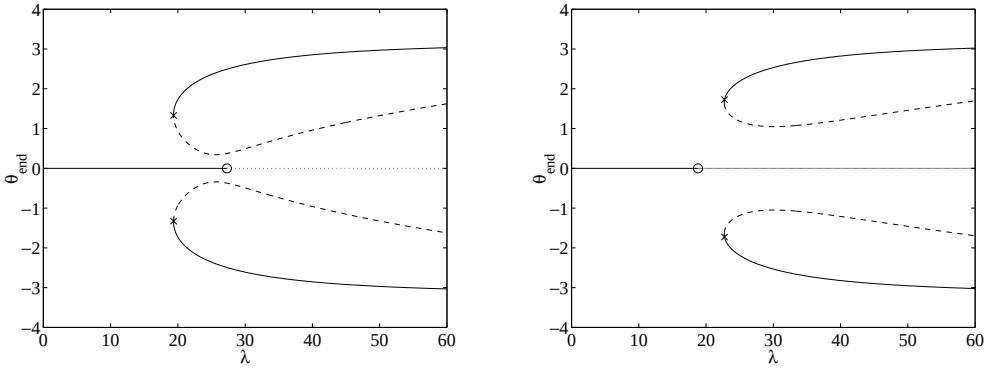

(e) $\mu = 10.0$ (f) $\mu = 12.0$

Figure 4.4. *For $\alpha = 0.0$ and $\gamma = 1.0$. A value characteristic of our entire solution θ_{end} is plotted as a function of λ for a variety of f. The full, dashed, and dotted lines represent stable solutions, solutions with one unstable mode, and doubly unstable solutions, respectively. Square, circle, and X markers are used to denote a pitchfork bifurcation, Hopf bifurcation, and turning point, respectively. Each bifurcation diagram was selected to represent a significant section of Figure 4.3. As the dimensionless follower force increases, the two pitchfork bifurcation points tend toward each other until they coalesce, leaving a Hopf bifurcation and two turning points in their wake.*

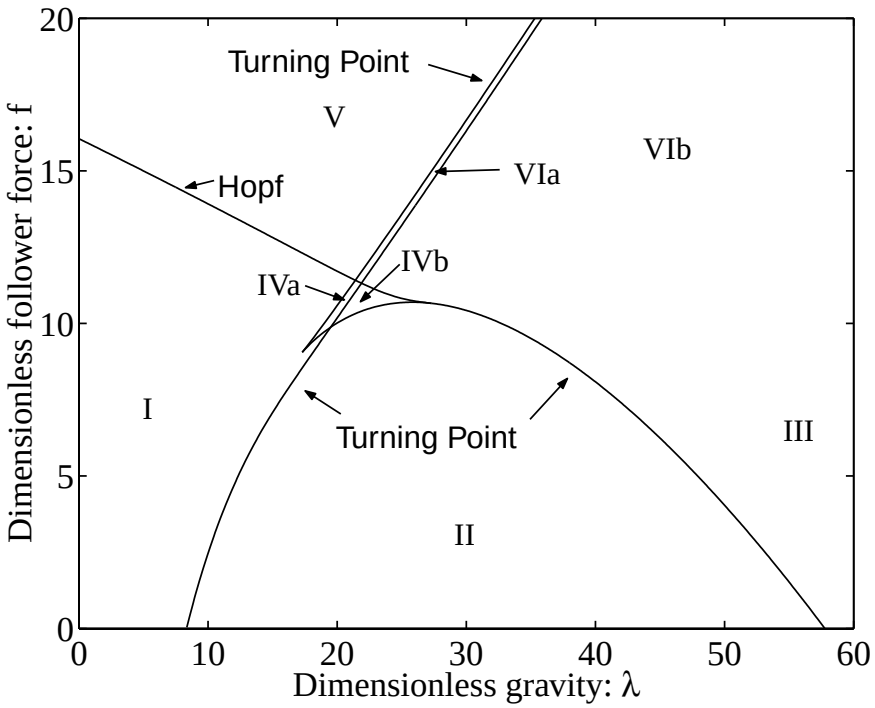

I. one near-symmetric/buckled solution
II. two buckled solutions
III. two buckled solutions
IVa. one near-symmetric and one buckled solution
IVb. one near-symmetric and two buckled solutions
V. one oscillatory solution
VIa. one oscillatory and one buckled solution
VIb. one oscillatory and two buckled solutions

Figure 4.5. *For $\alpha = 0.0125$ and $\gamma = 1.0$. When we break the symmetry by the introduction of a deflection $\alpha = 0.0125$, we obtain the following two-parameter plot. Notice that the curve of pitchfork bifurcations splits into two curves of turning points. The region of stability* (I) *does not appear to have increased dramatically. The near-symmetric/buckled modifier implies a solution which continuously transitions from a stable, almost symmetric solution to a buckled solution.*

points which appear in Figure 4.3. It should be noted that there are two curves of turning points shown in Figure 4.3 which happen to lie on the same curve in parameter space. Before we unfold these two higher codimension bifurcation points in α, we will highlight the effect the dimensionless follower force, gravity, and damping have on the boundaries of instability.

As can be seen in Figure 4.3, gravity makes the beam more likely to flutter and hence destabilizes the beam. This result agrees with our physical intuition that gravity is a force tending to make the beam oscillate. Contrary to physical intuition, the follower force μ makes the beam less likely to buckle and hence stabilizes the beam. This apparent paradox can be explained in the following way: if the beam is perturbed in the direction of its buckled state,

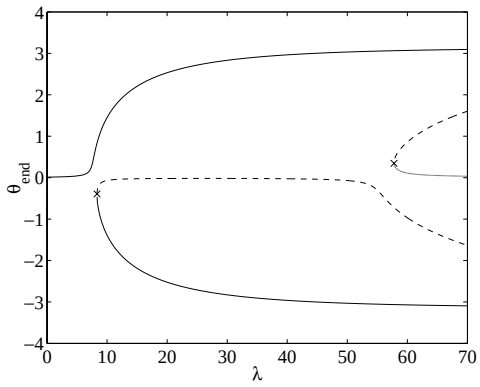

(a) $\mu = 0.0$

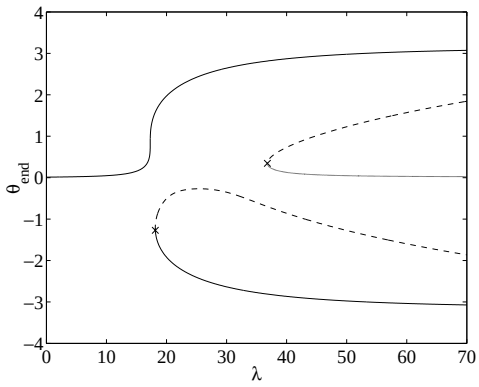

(b) $\mu = 9.05$

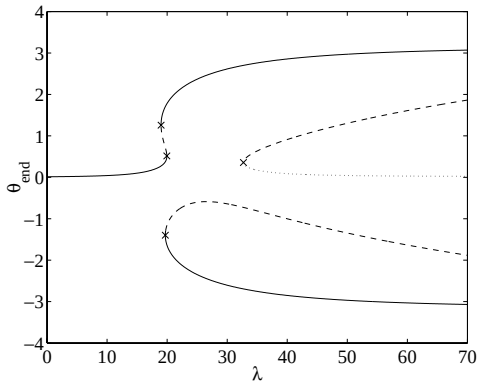

(c) $\mu = 10.0$

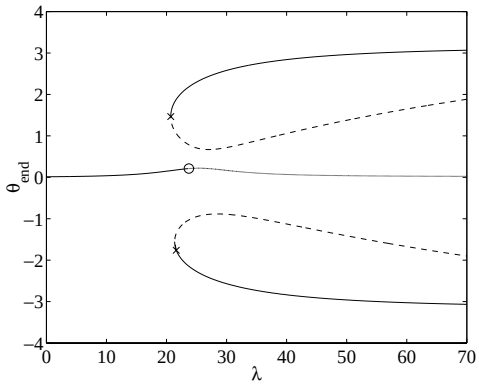

(d) $\mu = 11.0$

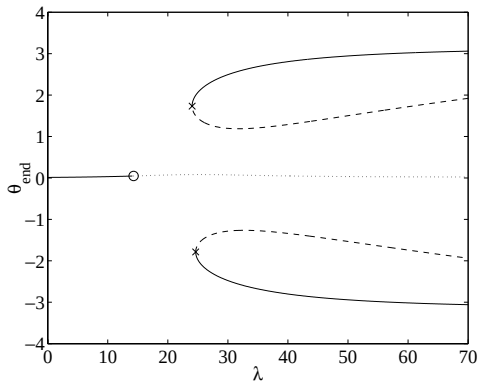

(e) $\mu = 13.0$

Figure 4.6. *For $\alpha = 0.0125$ and $\gamma = 1.0$. A value characteristic of our entire solution θ_{end} is plotted as a function of λ for a variety of f. The full, dashed, and dotted lines represent stable solutions, solutions with one unstable mode, and doubly unstable solutions, respectively. A circle and X symbols are used to denote a Hopf bifurcation and turning point, respectively.*

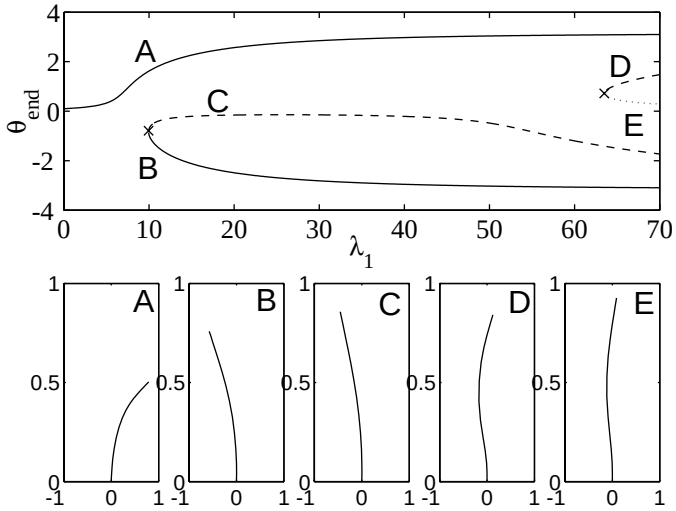

Figure 4.7. *For $\alpha = 0.1$ and $\gamma = 1.0$. The full and dashed lines represent stable and unstable solutions, respectively, and the X marker indicates a turning point. Clearly the solution corresponding to* A *is favored over solutions on branch* B*. The same pattern holds for the rest of the bifurcation diagram which corresponded to the second pitchfork bifurcation point in the symmetric case shown in Figure 4.1.*

then the follower force tends to push the beam back to the standing cantilever fixed point. The effect of the follower force agrees with Païdoussis' result that standing cantilevers which would ordinarily buckle without flow can actually become more stable with flow for a certain range of flow rates [15].

The follower force, however, also appears to excite the second pitchfork bifurcation mode by decreasing the critical value of λ, marking the onset of the second pitchfork instability. This phenomenon is apparent in bifurcation diagrams (a) and (b) in Figure 4.4. These bifurcation diagrams plot a characteristic value of our solution, the angle at the end of the beam, as a function of λ for fixed μ.

Bifurcation diagram (b) in Figure 4.4 marks the quartic bifurcation point—the transition between a supercritical and a subcritical pitchfork bifurcation. This point corresponds to the intersection of the turning point curves and the pitchfork bifurcation curve in Figure 4.3. The pitchfork bifurcation becomes subcritical because the branched solutions are unstable and occur when the symmetric solution is stable.

As the value of μ continues to increase, we notice the emergence of the Hopf bifurcation point in bifurcation diagram (d) in Figure 4.4. The second mode of instability becomes so excited by the increased follower force and the first mode so subdued by the stabilizing effect of the follower force that the two points coalesce at the higher codimension bifurcation point, where the Hopf bifurcation curve intersects the curve of pitchfork bifurcation points. As can be seen in bifurcation diagram (e), a Hopf bifurcation and two turning points remain in their wake. At a sufficiently high follower force, the Hopf bifurcation emerges as the first instability the symmetric system experiences as λ is increased. Bifurcation diagram (f) in Figure 4.4 shows that two turning points still remain, but the buckled solutions no longer coexist with a stable symmetric solution.

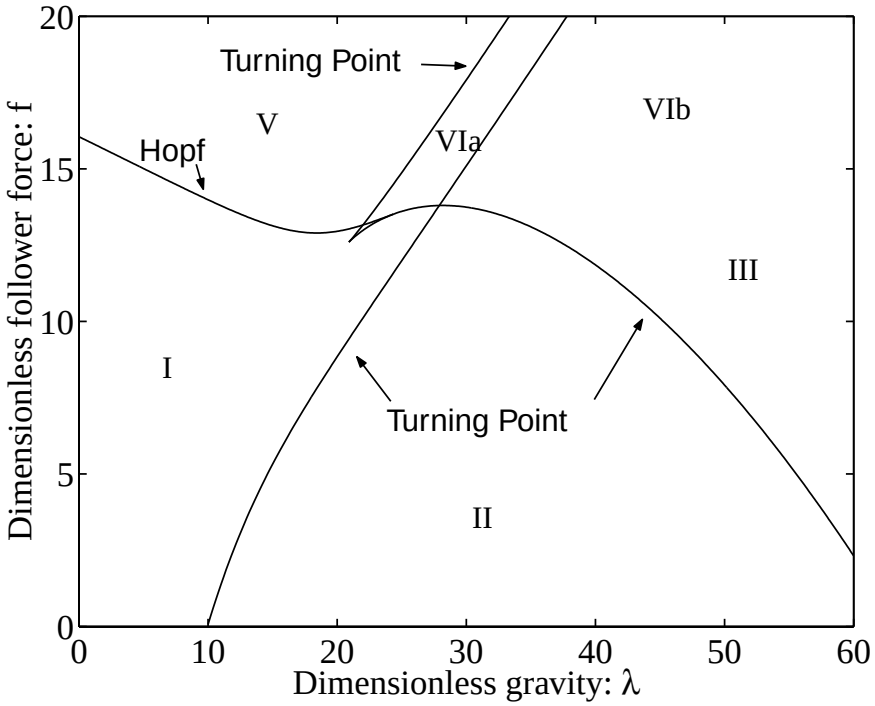

I. one near-symmetric/buckled solution
II. two buckled solutions
III. two buckled solutions
IV. one near-symmetric/buckled and two buckled solutions
V. oscillatory solution
VIa. one oscillatory and one buckled solution
VIb. one oscillatory and two buckled solutions

Figure 4.8. *For $\alpha = 0.1$ and $\gamma = 1.0$. Each region indicated with a Roman numeral and demarcated by the curves of bifurcation points has different stable solutions outlined above. The near-symmetric solution continuously transitions from a slightly deflected solution to a buckled solution in region* I *but never experiences a turning point or bifurcation.*

For $\lambda = 0$, without damping, the standing cantilever was neutrally stable up until $\mu = 20.0$, where the beam experienced flutter. With a small amount of damping, γ, the beam experienced flutter at a smaller value of μ, leaving us puzzled by the prospect that damping had a destabilizing effect on the beam. This important finding was also noted by others in the literature. However, a more puzzling consequence of our implementation of damping is that the Hopf bifurcation point is absolutely independent of γ. These puzzling results are explained in section 4.3.

The series of bifurcation diagrams in Figure 4.4 are used to define the regions in Figure 4.3 by the type of stable solutions which exist. Region I indicates that all solutions tend toward the standing cantilever fixed point. In Region II, the symmetric fixed point loses stability to one of the buckled branches depending on the direction of the perturbation. This scenario

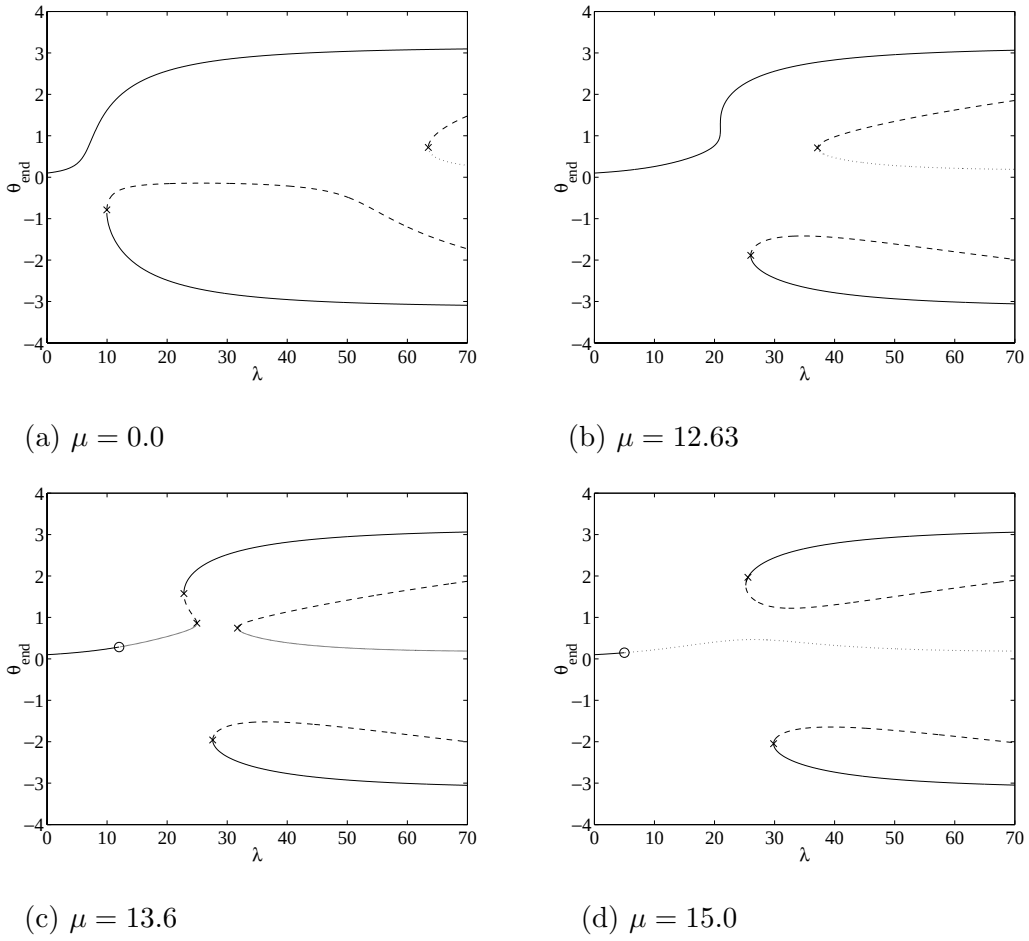

Figure 4.9. $\alpha = 0.1$. *A value characteristic of our entire solution θ_{end} is plotted as a function of λ for a variety of f. The full, dashed, and dotted lines represent stable solutions, solutions with one unstable mode, and doubly unstable solutions, respectively. A circle and X symbols are used to denote a Hopf bifurcation and turning point, respectively.*

remains true even after the second pitchfork bifurcation point is passed in Region III. The symmetric and buckled solutions are all stable in Region IV. It should be noted that the two-parameter plot can be misleading because it contains bifurcations of different solutions on the same parameter space. In order to correctly interpret Figure 4.3, please view the one-parameter plots in Figure 4.4. It should also be noted that Regions VI and V do not have well-defined boundaries in Figure 4.3. Region VI has only oscillatory solutions, while, in Region V, both steady and oscillatory solutions are stable. LOCA cannot predict the end of the oscillatory solutions that occurs when the limit cycle has a period which reaches ∞ and ceases to exist. Time-integration of the governing equations of the motion of the beam is one way to obtain this boundary.

What happens to the two higher codimension bifurcation points as we unfold them in α? The authors were unable to locate any work that discussed the unfolding of these higher

codimension bifurcation points in α. When we deflect the beam slightly ($\alpha = 0.0125$), we obtain the two-parameter plot shown in Figure 4.5. We notice that the curve of pitchfork bifurcations has given rise to two curves of turning points. The quartic bifurcation point has unfolded into a codimension two bifurcation, where a curve of turning points terminates at a cusp, and a codimension one bifurcation corresponding to the remaining curve of turning points. The intersection of the Hopf bifurcation and the pitchfork bifurcation curves has unfolded into a double zero eigenvalue which marks where the Hopf bifurcation curve intersects the curve of turning points in Figure 4.5. The effects of unfolding become more pronounced as we continue to increase the deflection as seen in Figure 4.8. We will briefly highlight some features of the deflected beam.

With a small deflection, rather than either branched solution being equally possible, stability appears to be biased toward the direction of the deflection. In fact, the solution in the direction of the deflection is stable for the deflected case. This bias becomes especially evident in the bifurcation diagrams shown in Figure 4.6.

Bifurcation diagram Figure 4.6 (a) clearly shows that one stable solution branch connects the standing cantilever and one of the buckled branches. Buckling in this case is a continuous transition and is not characterized by a bifurcation. The near-vertical standing cantilever equilibria become disconnected from the unstable near-standing solution, which is typical of how a pitchfork bifurcation diagram looks after the symmetry is broken. The second pitchfork bifurcation mode behaves as expected as well when the symmetry is broken. As we increase the dimensionless follower force, we arrive at the cusp shown in Figure 4.5. Similar to the symmetric case, the second turning point moves closer to the stable branches, until the stable deflected branch merges with the second turning point, leaving a Hopf bifurcation point. By the time $\mu = 13$ in bifurcation diagram (e), we notice that the Hopf bifurcation point becomes the first instability the near-symmetric solution experiences.

For larger deflections ($\alpha = 0.1$), Figure 4.7 shows how the beam actually looks as we move on the various stable, unstable, and doubly unstable solution branches. Notice that the solution in the direction of the deflection is stable and clearly favored over the solution on the turning point branch. The two-parameter plot for the $\alpha = 0.1$ case is shown in Figure 4.8. The bifurcation diagrams shown in Figure 4.9 are again revealing. Bifurcation diagram (a) shows that the solution corresponding to the direction opposing the direction of the deflection is unfavored and disconnected from the near-symmetric solution. The near-symmetric solution is initially stable and remains stable even as it becomes more deflected and loses more symmetry. This stability is due to the continuous nature of the transition from the near-symmetric solution to what we would consider a buckled solution. As the dimensionless follower force increases, we notice that the second turning point moves closer to the stable solution branch. By the time $\mu = 13.6$, the beam can flutter. The beam, however, restabilizes and continues on the deflected solution branch. The second pair of turning points then merges, leaving a Hopf bifurcation in its wake.

4.2. The quartic bifurcation point. By applying the theory of normal forms, we can obtain a one-dimensional equation which can validate the topological behavior of the two-parameter plots we obtained in the neighborhood of the quartic bifurcation point we noticed in Figure 4.3. At this point, the beam exhibits symmetry, and, because we are at a transition

between a subcritical and a supercritical pitchfork bifurcation, we can ignore terms of order greater than five in x (since $F_{xxx} = 0$). We will introduce parameters (a, b) such that, at the quartic bifurcation point, $a = b = 0$. The one-dimensional equation which represents the basic topological behavior in the vicinity of a quartic bifurcation point follows:

$$g(x) = \pm x^5 + ax^3 + bx = 0, \tag{4.1}$$

where a and b are parameters which we can vary in this equation. This normal form is a standard example in the work of Golubitsky and Schaeffer [11]. We will choose the sign in front of the quintic term in (4.1) to be negative because the resulting equation better resembles the topological behavior in Figure 4.3. The solution, $x = 0$, corresponds to the symmetric solution. Furthermore, for any given value of a, $b = 0$ corresponds to the locus of pitchfork bifurcation points, where $\frac{\partial g}{\partial x}(0) = 0$. Also notice that, for $a < 0$, the pitchfork bifurcation point is supercritical and, for $a > 0$, the pitchfork bifurcation point is subcritical.

We are interested in seeing if there are any curves of turning points in the neighborhood of this quartic bifurcation point. By definition, at a turning point, the following is true:

$$\frac{dg}{dx}(x) = -5x^4 + 3ax^2 + b = 0. \tag{4.2}$$

Neglecting the trivial solution which corresponds to the locus of pitchfork bifurcation points, we can solve (4.1) and (4.2) to obtain an expression for the locus of turning points near the quartic bifurcation:

$$\frac{a^2}{4} + b = 0, \qquad x^2 = \frac{a}{2}.$$

A schematic of b as a function of a is given in Figure 4.10. Notice the locus of turning points comes tangent to the locus of pitchforks and terminates at the quartic bifurcation point. Also notice that the curve of turning points is actually two curves of turning points which happen to lie on the same curve in parameter space and correspond to the two different solutions: $x = \pm\frac{\sqrt{a}}{\sqrt{2}}$. This topological behavior is seen in Figure 4.3.

Figure 4.5 shows how the quartic bifurcation point unfolds when we break the symmetry in the beam equations. There are two notable features in the unfolding: a curve of turning points which terminates at a cusp and another curve of turning points nearby. Let us now show that, when we break the symmetry in the normal form (4.1), we also obtain these features. The asymmetric normal form follows:

$$g(x) = -x^5 + ax^3 + dx^2 + bx + c = 0. \tag{4.3}$$

We begin by looking for a cusp. When $d = 0$, the conditions for a cusp can be written as

$$\begin{aligned} g(x) &= -x^5 + ax^3 + bx + c = 0, \\ \frac{dg}{dx}(x) &= -5x^4 + 3ax^2 + b = 0, \\ \frac{d^2g}{dx^2}(x) &= -20x^3 + 6ax = 0. \end{aligned}$$

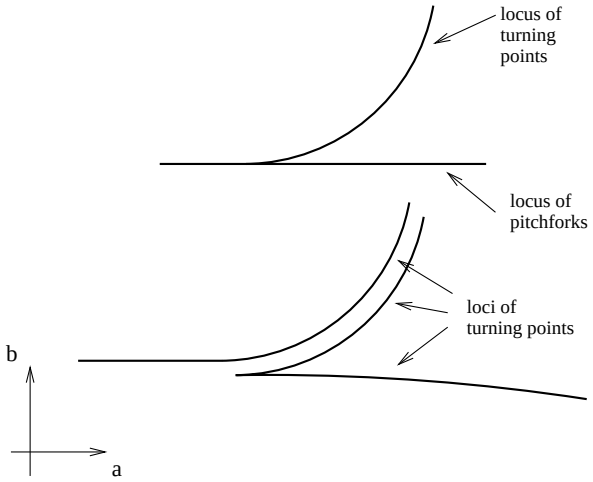

Figure 4.10. *From the top: A schematic of the locus of turning points near the quartic bifurcation point and a schematic of the locus of turning points after the symmetry is broken. The top schematic agrees with the topological behavior in the neighborhood of the quartic bifurcation point in Figure 4.3. The bottom schematic agrees with Figure 4.5, which shows the unfolding of the quartic bifurcation point.*

Solving these equations we obtain $a = \frac{5|c|^{2/5}}{2^{1/5}3^{3/5}}$, $b = -\frac{3^{7/5}|c|^{2/5}}{4\cdot 2^{1/5}}$, and $x = \frac{3^{2/5}|c|^{2/5}}{2^{6/5}}$. Thus, for each value of c with $d = 0$, there is one and only one cusp. For $d \neq 0$, we can invoke the implicit function theorem to conclude that, for small d, this conclusion still holds.

In the symmetric normal form, we noticed that two curves of turning points happened to lie on the same curve in parameter space. When we break the symmetry, these curves of turning points split apart in parameter space, as shown in Figure 4.10. One of these curves terminates at a cusp, and the other is a locus of turning points that continues on and merges into what used to be the supercritical pitchforks.

4.3. Effect of damping. When $\gamma = 0.0$, we noted in section 2.4 that the eigenvalue problem obtained from linearizing about the standing cantilever fixed point could only predict neutral stability or instability. In section 4.1, we found that, at $\mu = 20.0$, the beam experiences flutter. For $\mu < 20.0$, the neutrally stable modes do not necessarily tell us anything about the stability of the standing cantilever. One would assume that, when we add damping, those neutrally stable modes would become stable. We noticed numerically, however, that damping made some of those neutrally stable modes unstable. In addition, we analyzed the effect damping had on this point of instability by introducing extreme values of damping ($\gamma = 10^{-5}$ and $\gamma = 10^{5}$) and observed that damping had no effect on this point of instability. These deeply puzzling results are analytically clarified in this section.

By applying the perturbation theory of eigenvalues, we can determine the effect a small amount of damping would have on the sign of the real part of the perturbation in the eigenvalue. If the real part of the perturbation is positive, then the damped solution becomes unstable, and, if the real part of the perturbation is negative, then we know the solution will

become stable. Assuming γ is small, let us introduce the following expansions for this purpose:

$$\begin{aligned}\phi &= \phi_0 + \gamma\phi_1,\\ \sigma &= \sigma_0 + \gamma\sigma_1.\end{aligned}$$

Substituting these expansions into (2.6) and collecting terms up to first-order in γ, we obtain

$$\begin{aligned} L(\phi_1) + \sigma_0^2\phi_1 &= -2\sigma_0\sigma_1\phi_0,\\ \phi_1(0) = \phi_1'(0) &= 0,\\ \phi_1''(0) &= 0,\\ \phi_1'''(1) &= \sigma_0\phi_0(1).\end{aligned} \tag{4.4}$$

Using Fredholm's alternative, we can take the inner product of both sides of the first equation in (4.4) with ψ_0, which satisfies the linear operator in (2.8) and the adjoint boundary conditions in (2.9). Repeatedly integrating this resulting equation by parts, we can then apply the boundary conditions in ϕ_0 and use the fact that $L\psi_0 + \sigma_0^2\psi_0 = 0$ to obtain the following equation:

$$\psi_0(1)\sigma_0\phi_0(1) = -2\int_0^1 \psi_0\sigma_0\sigma_1\phi_0 ds.$$

Finally, solving for σ_1, we obtain

$$\sigma_1 = -\frac{\psi_0(1)\phi_0(1)}{2\int_0^1 \psi_0\phi_0 ds}. \tag{4.5}$$

When there is no follower force ($\mu = 0$ and hence $\phi_0 = \psi_0$), σ_1 is negative. Therefore, a little bit of damping stabilizes the standing cantilever when there is no follower force. For small μ, we would expect σ_1 to remain negative since $\phi_0 \approx \psi_0$. As we increase μ, we can solve the purely inviscid problem and keep track of the undamped right and left eigenfunctions to obtain the point where a small amount of damping makes the standing cantilever unstable. σ_1 changes sign when $\psi_0(1)$, $\phi_0(1)$, or the denominator changes sign. Numerically, we have identified that $\psi_0(1)$ changes sign when $\mu = 16.0$. This important result proves that a point source of damping destabilizes the beam.

We have shown that an instability occurs for small values of γ at $\mu = 16.0$ and $\psi_0(1) = 0.0$. However, why does this point of instability hold for all values of γ? How can we explain this special property of the point source of damping in our model of the beam? Since $\psi_0(1) = 0$ at the point of instability, one of the adjoint boundary conditions in (2.9) becomes

$$\psi_0''(1) = 0.$$

Therefore, both ϕ_0 and ψ_0 satisfy all of the boundary conditions for the damped problem at the point of instability except for $\phi'''(1) = \sigma_0(1)\phi_0(1)$. We can thus obtain an eigenfunction which satisfies the damped linear operator and boundary conditions using a linear combination of the undamped left and right eigenfunctions ϕ_0 and ψ_0. Since we can determine an eigenfunction $\phi^d(\gamma)$ for the damped linear operator in (2.6) that ensures that the eigenvalue

remains unchanged as we vary γ, we have proven that the point of instability is independent of damping. It turns out that this particular linear combination is

$$\phi = \phi_0 + k\gamma\sigma_0\psi_0,$$

where $k = -\frac{\phi_0(1)}{\mu\psi_0'(1)}$.

We have shown that, as long as a point source of damping is nonzero, damping has no effect on the Hopf bifurcation point. It should be emphasized that this is an interesting property of what is most probably a degenerate model and does not hold for distributed damping or even two point sources of damping for that matter. However, just as we learned a tremendous amount from the extremely degenerate high codimension bifurcations, we hypothesize that this degenerate point foretells that distributed damping would have a nominal effect on the point of instability. Our hypothesis is strengthened by the work of Païdoussis, who showed in Table 2 of his paper that the effect external distributed damping had on the critical flow velocity for the standing cantilever is small [15]. A more physical explanation of why damping actually destabilizes the beam follows, culminating in a discussion that restates conclusions made by Benjamin about the physical mechanism behind flutter [4].

4.4. Physical mechanism behind flutter. Let us assume that $\sigma = i\omega$. By construction, a fixed point of the beam takes the form

$$\mathbf{x} = \Re(\phi_1 e^{i\omega t}),$$

where ϕ_1 is the eigenfunction of the linear operator appearing in (2.6). The work performed by the follower force is approximately

$$W = \mu \int_0^t u(1)\theta(1)dt.$$

We stated in section 2.4 that, when we linearize about the standing cantilever fixed point, we obtain a fourth-order differential equation in x, and we used ϕ_1 to denote the eigenfunction. For small deflections, θ is simply equal to ϕ_1' since, in (2.4), $x' = \sin(\theta)$. Putting this all together, $u(1)$ and $\theta(1)$ have the following form:

$$\begin{aligned} u(1) &= \Re(i\omega\phi_1(1)e^{i\omega t}), \\ \theta(1) &= \Re(\phi_1'(1)e^{i\omega t}). \end{aligned}$$

Without loss of generality, we can normalize the eigenfunction ϕ_1 such that

$$\begin{aligned} \phi_1(1) &= 1, \\ \phi_1'(1) &= Ae^{i\beta}, \end{aligned}$$

where A and β are real constants obtained after normalizing the eigenfunction so that $\phi_1(1) = 1$. The u velocity and θ in terms of this normalized eigenfunction are

$$\begin{aligned} u(1) &= -\omega\sin(\omega t), \\ \theta(1) &= A\cos(\omega t + \beta), \end{aligned}$$

so that the work performed by the follower force can be expressed as

$$W = -\mu \int_0^t \omega A \sin(\omega t) \cos(\omega t + \beta) dt.$$

This integral evaluates to zero over a full period, unless β is nonzero. When there is no damping $\gamma = 0$, then ϕ_1 and ϕ_1' are real and β is zero. Essentially, there is no energy transfer from the follower force to the beam when there is no damping. When there is damping, β becomes nonzero because ϕ_1 and ϕ_1' become complex. This energy due to the follower force is countered by the energy removed from the system by dissipation. At a certain point, the follower force outweighs the damping mechanism, causing the beam to become unstable. Thus the beam experiences an instability because the u velocity and θ become more in phase. These results are consistent with those found by Benjamin [4].

5. Conclusion. As a result of this research, we have outlined the development of a generic tool for detecting the criticality of a pitchfork bifurcation point. In the future, we will want to develop this tool for large-scale stability problems. Moreover, because a point source of damping had no influence on the Hopf bifurcation point, we predicted that distributed damping would have a nominal effect on stability. We would like to test the validity of this claim by implementing global damping in future work. In this study, we used α only to unfold our high codimensional pitchfork bifurcations. Future work may consider α as a continuation parameter and examine bifurcations in α. We may also wish to identify the saddle-loop bifurcation curve missing in our two-parameter plot by time-integrating our equations of motion.

Acknowledgments. We thank Jerry Marsden and Simon Tavener for their help with this paper. We also thank Danny Sorensen and Richard Lehoucq for making this research opportunity available to the authors.

REFERENCES

[1] A. K. Bajaj, P. R. Sethna, and T. S. Lundgren, *Hopf bifurcation phenomena in tubes carrying a fluid*, SIAM J. Appl. Math., 39 (1980), pp. 213–230.

[2] A. K. Bajaj and P. R. Sethna, *Flow-induced bifurcations to three-dimensional oscillatory motions in continuous tubes*, SIAM J. Appl. Math., 44 (1984), pp. 270–286.

[3] A. K. Bajaj and P. R. Sethna, *Effect of symmetry-breaking on flow-induced oscillations in tubes*, J. Fluids and Structures, 5 (1991), pp. 651–679.

[4] T. B. Benjamin, *Dynamics of a system of articulated pipes conveying fluid.* I. *Theory*, Proc. Roy. Soc. Ser. A, 261 (1961), pp. 457–486.

[5] T. B. Benjamin, *The threefold classification of disturbances in flexible surfaces bounding inviscid flows*, J. Fluid Mech., 16 (1963), pp. 436–450.

[6] W. J. Beyn, *Numerical analysis of homoclinic orbits emanating from Takens-Bogdanov point*, IMA J. Numer. Anal., 14 (1994), pp. 381–410.

[7] A. M. Bloch, P. S. Krishnaprasad, J. E. Marsden, and T. S. Ratiu, *Dissipation induced instabilities*, Ann. Inst. H. Poincaré Anal. Non Linéaire, 11 (1994), pp. 37–90.

[8] A. M. Bloch, P. S. Krishnaprasad, J. E. Marsden, and T. S. Ratiu, *The Euler-Poincaré equations and double bracket dissipation*, Comm. Math. Phys., 175 (1996), pp. 1–42.

[9] C. Canuto, M. Y. Hussaini, A. Quarteroni, and T. A. Zang, *Spectral Methods in Fluid Dynamics*, Springer-Verlag, New York, 1988, pp. 7–9.

[10] K. A. Cliffe and A. Spence, *The calculation of high order singularities in the finite Taylor problem*, in Numerical Methods for Bifurcation Problems, Internat. Schriftenreihe Numer. Math. 70, Birkhäuser, Basel, 1984, pp. 129–144.

[11] M. Golubitsky and D. G. Schaeffer, *Singularities and Groups in Bifurcation Theory*, Vol. I, Springer-Verlag, New York, 1985, p. 267.

[12] J. Guckenheimer and P. Holmes, *Nonlinear Oscillations, Dynamical Systems, and Bifurcations of Vector Fields*, Springer-Verlag, New York, 1983, pp. 290–295, 364–376.

[13] J. E. Marsden and J. Scheurle, *Lagrangian reduction and the double spherical pendulum*, Z. Angew. Math. Phys., 44 (1993), pp. 17–43.

[14] G. Moore and A. Spence, *The calculation of turning points of nonlinear equations*, SIAM J. Numer. Anal., 17 (1980), pp. 567–576.

[15] M. P. Païdoussis, *Dynamics of tubular cantilevers conveying fluid*, J. Mech. Engrg. Sci., 12 (1970), pp. 85–103.

[16] M. P. Païdoussis, *Fluid-Structure Interactions: Slender Structures and Axial Flow*, Academic Press, New York, 1998, pp. 111–132.

[17] M. P. Païdoussis and N. T. Issid, *Dynamics stability of pipes conveying fluid*, J. Sound Vibration, 33 (1974), pp. 267–294.

[18] M. P. Païdoussis and G. X. Li, *Pipes conveying fluid: A model dynamical problem*, J. Fluids and Structures, 7 (1993), pp. 137–204.

[19] G. Pfister, H. Schmidt, K. A. Cliffe, and T. Mullin, *Bifurcation phenomena in Taylor-Couette flow in a very short annulus*, J. Fluid Mech., 191 (1988), pp. 1–18.

[20] A. G. Salinger, N. M. Bou-Rabee, E. A. Burroughs, R. B. Lehoucq, R. P. Pawlowski, L. A. Romero, and E. D. Wilkes, *LOCA* 1.0: *Library of Continuation Algorithms, Theory and Implementation Manual*, Sandia Technical Report SAND2002-0396, Sandia National Laboratories, Albuquerque, NM, 2002, available online from http://www.cs.sandia.gov/LOCA.

[21] A. G. Salinger, R. B. Lehoucq, R. P. Pawlowski, and J. N. Shadid, *Computational bifurcation and stability studies of the* 8:1 *thermal cavity problem*, Internat. J. Numer. Methods Fluids, to appear.

[22] C. Semler, G. X. Li, and M. P. Païdoussis, *The non-linear equations of motion of pipes conveying fluid*, J. Sound Vibration, 169 (1994), pp. 577–599.

[23] S. W. Shaw and P. R. Sethna, *On the effects of asymmetries on a system near a codimension two point*, in Dynamical Systems Approaches to Nonlinear Problems in Systems and Circuits, F. M. A. Salam and M. Levi, eds., SIAM, Philadelphia, 1988, pp. 317–332.

[24] S. W. Shaw and P. R. Sethna, *On codimension-three bifurcations in the motion of articulated tubes conveying a fluid*, Phys. D, 24 (1987), pp. 305–327.

[25] B. Werner and A. Spence, *The computation of symmetry-breaking bifurcation points*, SIAM J. Numer. Anal., 21 (1984), pp. 388–399.

[26] W. Wu, A. Spence, and K. A. Cliffe, *Steady-state Hopf mode interaction at a symmetry-breaking Takens-Bogdanov point*, IMA J. Numer. Anal., 14 (1994), pp. 137–160.